Efficiency of the differential absorption lidar methods under cloudy atmospheric conditions

G.M. Krekov and M.M. Krekova

Institute of Atmospheric Optics,
Siberian Branch of the Russian Academy of Sciences, Tomsk

Received July 14, 2005

Reduction of systematic lidar measurement errors due to differential attenuation and backscattering by aerosol and cloud particles is a key problem in determination of atmospheric ozone concentration. In the framework of the method of statistical tests, a comparative analysis of the efficiency of different algorithms of the differential absorption lidar (DIAL) technique for cases of elastic and inelastic scattering has been performed. The algorithms include the canonical DIAL technique, in which the ozone concentration profile is calculated using ratio of two signals measured at on- and off-line wavelengths within an absorption band. We consider specific features of the classical Raman method and of a new rotational-vibrational method. It is shown that the wavelength-dependent multiple scattering and the differential absorption by cloud particles are the principal sources of systematic errors in the ozone measurements, which dictates the necessity of their correction.

Introduction

Our previous work[1] addressed some questions on the efficiency of the methods of rotational-vibrational Raman spectroscopy in laser sensing of a cloudy atmosphere. In that paper we have presented estimates of the potential accuracy achievable in retrieving the vertical profiles of temperature and humidity under conditions of interference from multiple scattering noise in the Raman sensing channels. In addition to temperature and humidity, the ozone is also an important meteorological parameter determining the chemical and thermodynamic structure of the Earth atmosphere. The field studies of atmospheric ozone have been performed for several decades using diverse types of the instrumentation. Generalization of the available results as well as of the regularities revealed in the global ozone distribution has been the subject of many publications including Ref. 2. Quite comprehensive databank has been compiled on the ozone measurements, which enables one not only to reproduce the vertical profiles of the ozone by the methods of statistical simulation, but also to identify regional features in them.[3]

From this point of view, even more surprising is the fact that a number of works devoted to comparison of satellite sensing data such as part of the Limb Infrared Monitor of the Stratosphere (LIMS) and Solar Mesosphere Explorer (SME) programs[2,4,5] with the measurement results and model calculations reveal discrepancies in the reconstructed vertical profiles of O_3. The discrepancies are quite significant to become a subject of special discussion such as in this paper.

Some authors relate the possibility of explaining this fact with search for additional (besides the traditional[2] $N_2O + (^1D) \rightarrow NO + NO$) sources of nitrogen oxides at altitudes of the ozone maximum. However, no serious proofs of this assumption are available yet. On the other hand, a number of reports at the last International Laser Radar Conference (ILRC-2004)[6] attract attention to a significant relationship between spatial ozone stratification and aerosol and cloud layers in the upper troposphere and stratosphere. These conclusions follow both from model calculations[7,8] and *in situ* experimental measurements.[9]

It is important to remember that, in addition to heterogeneous chemical activity, the cloud and aerosol particles are also sources of active optical noise in the ozone sensing by photometric and lidar methods. This noise biases the estimates of vertical concentration profiles, especially in satellite measurements.[10] Now, when the tendency becomes urgent for the existing world network of lidar stations to evolve to routine mode of monitoring, prognosis of the noise-immunity of lidar methods under conditions of time-varying optical weather including clouds acquires special importance. Studies in this field are still few, nevertheless we should mention a number of works.[10–12] By making use of the results obtained in these studies we, naturally, will confine ourselves to the cases of upper-level clouds and possible aerosol inversions in the troposphere and stratosphere.

1. Vertical profiling of the ozone by differential absorption lidar (DIAL) method

Theoretical grounds of the DIAL method as applied to lidar measurements of the spatial humidity

0235-6880/05/10 812-10 $02.00

distribution in the atmosphere were formulated and implemented in practice by Schotland[13] yet in 1964. The idea behind this method was the spatial differentiation of the ratio of lidar returns at two closely spaced wavelengths around one of the H_2O absorption lines. The idea was found to be applicable to sensing of any constituents of the molecular (and sometimes aerosol) atmosphere, possessing resolved absorption spectra, including ozone possessing pronounced spectral behavior in the Hartley–Huggins UV bands.[14] However, the technical difficulties in the design of efficient UV lidars have postponed obtaining first valuable results on O_3 in the real atmosphere.[15] Presently, in the world network there are more than ten successively operating stationary lidar stations.[3,16] New methodical features in interpretation of lidar returns in the framework of DIAL method permanently appear.

Godin et al.[17] and Fiorani and Durieux[18] performed comparative analysis of noise-immunity of the methods used such as one developed for the forthcoming satellite sensing project.[19] They note that the canonical (elastic-DIAL) sensing scheme provides adequate results for limited altitude range $\Delta h \cong 10$–40 km, covering the stratosphere and upper troposphere under conditions of clear unperturbed atmosphere, more often at night. Under overcast cloud conditions, the measurements are impossible, because the presence even sparse cloudiness or aerosol inversions leads to uncontrolled bias of the results.[19,20] What is the main cause of the bias? The algorithm of DIAL implementation mathematically is very simple.

The lidar return from cloud and aerosol particles, as well as from air molecules, is described, in the single scattering approximation, by the well-known lidar equation

$$P(\lambda_i,h) = P_0(\lambda_i)\xi(h)\frac{\beta_\pi(\lambda_i,h)}{h^2}\exp\left[-\int_0^h \sigma(\lambda_i,h')\mathrm{d}h'\right], \quad (1)$$

where λ_i is the set of working wavelengths ($i = 0, 1, 2$); $P_0(\lambda_i)$ and $P(\lambda_i)$ are, respectively, the pulse power of sounding radiation and the optical power of a lidar return; $\xi(h)$ is the instrumental factor including the overlap function; $\sigma(\lambda_i, h)$ is the total atmospheric extinction coefficient; and $\beta_\pi(\lambda_i, h)$ is the volume backscattering coefficient. In the DIAL method, the extinction coefficient is usually represented as the sum

$$\sigma(\lambda_i,h) = \sigma_{\mathrm{ext}}(\lambda_i,h) + \sigma_{O_3}(\lambda_i,h), \quad (2)$$

where $\sigma_{O_3}(\lambda_i,h)$ is the absorption coefficient of the studied atmospheric gas, O_3 in this case; $\sigma_{\mathrm{ext}}(\lambda_i, h)$ is the extinction coefficient, which includes all other losses of laser radiation with the wavelength λ_i due to scattering, absorption, and reemission. In its turn,

$$\sigma_{O_3}(\lambda_i,h) = N_{O_3}(h)K(\lambda_i), \quad (3)$$

where $N_{O_3}(h)$ is the altitude profile of the gas concentration sought; and $K(\lambda_i)$ is the absorption cross section. Usually, if N is in units of cm^{-3}, then $K(\lambda)$ is in cm^2. Taking into account expressions (2) and (3), the solution of system of equations (1) for the trivial case ($i = 1$, $\xi(h) = 1$) leads to the well-known relation in the form of logarithmic derivative:

$$N_{O_3}(h) = \frac{1}{2\Delta K}\left\{\frac{\mathrm{d}}{\mathrm{d}h}\left[\ln\frac{P(\lambda_0,h)}{P(\lambda_1,h)}\right] + A + B\right\}, \quad (4)$$

where

$$A = -\frac{\mathrm{d}}{\mathrm{d}h}\left[\ln\frac{\beta_\pi(\lambda_0,h)}{\beta_\pi(\lambda_1,h)}\right]; \quad (5)$$

$$B = -2\left[\sigma_{\mathrm{ext}}(\lambda_0,h) - \sigma_{\mathrm{ext}}(\lambda_1,h)\right]; \quad (6)$$

$\Delta K = K(\lambda_0) - K(\lambda_1)$ is the differential frequency-averaged absorption coefficient. The terms A and B, strictly speaking, are not known, though the optical coefficients $\beta_\pi(\lambda)$ and $\sigma_{\mathrm{ext}}(\lambda)$ entering these quantities include molecular scattering contribution, which is more easy for prediction and estimation.

Some authors such as Uchino et al.,[19] Kovalev and McElroy[22] and Kovalev and McElroy,[23] simply neglect the influence of the term (5). Other researchers, such as Krekov and Zvenigorodskii,[2] Browell et al.,[20] Kovalev and McElroy,[21] and Bukreev et al.[24] argue that the uncertainty of A values is the main source of errors in retrieving the profile $N_{O_3}(h)$. In this regard, a number of algorithms has been proposed[12,21,24,25] to estimate the differential absorption by aerosol in the spectral region chosen. All of them suggest simultaneous solution, in one or another way, of the system of equations (1) for aerosol scattering coefficients. The solution is generally sought using the so-called Klett method. The Klett method, also called the method of integral accumulation with reference point at the end of the sounding path, was formulated in our earlier work,[26] where we also showed that this method is less stable under conditions of interference of the multiple scattering noise.

Zuev et al.[25] have suggested more efficient algorithm of solving the systems of equations of the type (1) for the sounding scheme with Raman-lidar-based measurements of the atmospheric molecular density. The algorithm relies upon integral processing of a digitized backscattering signal. The calculation scheme is readily extended to any multifrequency sensing scheme (see Appendix), including the case of DIAL method. Uncertainty in the estimated A factor in Eq. (4) can be totally removed by invoking the inelastic Raman scattering channels as suggested in Refs. 11, 12, and 30. The prospects of this approach under conditions of multiple scattering noise interference are assessed below.

2. Ideology of numerical experiments on laser sensing of atmospheric ozone

2.1. Accuracy characteristics of DIAL method

The accuracy characteristics of DIAL method as applied to measurements of the ozone vertical profiles in the earth atmosphere have been studied in a number of papers such as Refs. 2–6, 10–12, 17–22, and 30. A detailed review of earlier studies is given in monographs by Kostko et al.[22] and Measures.[31] It was found that the accuracy of the final estimate of the gas concentration is determined by: 1) fluctuations of the fields of signal and sky background at daytime (nighttime); 2) spectral, temporal, and spatial variations of the atmospheric backscatter and transmission; 3) space and time variations of temperature and pressure; 4) interference of nearby absorption bands of foreign gases; and 5) by misalignment between the sounding beam and the receiver's field of view, etc. Nonetheless, the canonic representations such as in Ref. 31 are generally restricted to just points (1) and (2); that is, the relative retrieval error of ozone concentration $\delta N_{O_3}/N_{O_3}$ within an arbitrary height interval Δh_j (we take $j = 1, 2$ for simplicity) in the case of the use of two wavelengths ($i = 1, 2$) is determined by

$$\varepsilon = \frac{\delta N_{O_3}}{N_{O_3}} = \frac{1}{2N_{O_3}\Delta K \Delta h} \times$$

$$\times \left\{ \sum_{i=1}^{2} \sum_{j=1}^{2} \left[\frac{\rho_\lambda (P_{ij} + P_b + P_d)}{n_{ik} P_{ik}^2} + \frac{\delta \beta_{ij}}{\beta_{ij}} \right] + \delta \tau_{ext} \right\}, \quad (7)$$

where we have introduced the simplifying notations:

$$P_{ij} = P(\lambda_i, h_j); \quad \beta_{ij} = \beta_\pi(\lambda_i, h_j).$$

In addition, $\Delta h = h_2 - h_1$; P_b, and P_d are the powers of passive background radiation and inherently instrumental noise, respectively; n_{ik} is a sample of the number of laser pulses; $\rho_\lambda = h_p c^2 / 2\lambda\eta\Delta h$; h_p is the Planck's constant; c is the speed of light; η is the quantum efficiency of a photodetector; and

$$\tau_{ext} = \int_{h_1}^{h_2} \sigma_{ext}(h) \mathrm{d}h'$$

is the optical depth of differential extinction due to all factors except the absorption by O_3.

Modern requirements to operation of lidar systems include the necessity of routine operation under complex conditions of optical weather.[38] The state of the atmosphere is characterized by the presence of about 80% of clouds including invisible ones.[11] Under these conditions, as was already noted in recent publications[1,10,11] and in a number of reports,[6] the set of actually significant factors entering into equation (7) should additionally include the active noise due to multiple scattering. Accordingly, formula (7) assumes the form

$$\varepsilon^* = \varepsilon + \delta\tau_{ms}, \quad (8)$$

where ε^* is the corrected estimate; and τ_{ms} is the optical depth due to multiple scattering. The quantity τ_{ms} is a nonlinear function of the total optical depth[32]:

$$\tau = \tau_{ext} + \int_0^h K(h') \mathrm{d}h'$$

and optical-geometrical sensing parameters including angular apertures of the receiver and transmitter, distance to the scattering medium, etc. To estimate τ_{ms}, it is necessary to solve complete nonstationary transfer equation; also, we know attempts to calculate τ_{ms} in two-stream approximation.[32]

2.2. Principles and model conditions of numerical experiment

The main principles of mathematical simulation in context of the study of influence of multiple scattering noise on the accuracy of $N_{O_3}(h)$ retrieval under different optical and geometrical conditions of sounding are as follows. In the equation (4), instead of single scattering signals $P(\lambda, h)$, we use the values of total signals

$$I(\lambda, h) = I_0(\lambda, h) + \Delta I_{ms}(\lambda, h),$$

normalized by the condition $I_0(\lambda, h) = P(\lambda, h)$; ΔI_{ms} is the multiple scattering contribution; and I_0 is the intensity of singly scattered signal. Accurate estimate of the functionals $I(\lambda, h)$ under conditions adequately fitting the numerical experiment is obtained by use of the Monte Carlo method. The main features of the algorithm of the method for solution of nonstationary transfer equation that includes inelastic (Raman) scattering effects were discussed in our earlier paper.[33] Here we only note some points associated with choice of the optical and technological conditions specific for DIAL sensing. We restrict ourselves to $N_{O_3}(h)$ sensing in the UV spectral region because in the IR absorption bands of O_3 the influence of within-cloud aerosol is less significant.

The choice of optimal wavelength pairs in the UV is limited, because of technological capabilities of the existing sources of radiation. Mainly, these are excimer lasers and Nd:YAG laser. The wavelengths used by different lidar research groups are presented in the table; more detailed comparative analysis can be found in Refs. 17, 34, and 35.

Wavelengths used in DIAL

Laser	Wavelength, nm	Lasing method	References
XeCl excimer	308	Fundamental frequency	3, 11, 12, 17, 24
	353	H_2-filled RC* (S_1)	
KrF excimer	248	Fundamental	24, 38
	268	D_2-filled RC (S_1)	
	277	H_2-filled RC (S_1)	
	292	D_2-filled RC (S_2)	
	313	H_2-filled RC (S_2)	
	266–341	(H_2 +D_2) -filled RC	
Nd : YAG	355	Fundamental x 3	11, 12, 17, 22, 30
	266	Fundamental x 4	
	289	D_2-filled RC (S_1)	
	299	H_2-filled RC (S_1)	
	316	D_2-filled RC (S_2)	
Dye	305–315	Rhodamine 590–610	18, 20, 37
	283–293		
Ti: Sapphire	290–300	Fundamental x 3	36

* H_2-filled RC (S_1) is hydrogen- (deuterium-) filled Raman cell, first Stokes scattering component.

Generally,[25,34,37,38] for simultaneous sensing of tropospheric and stratospheric aerosol the experimenters use complex lidar systems containing two optical channels: near UV ($\lambda < 300$ nm) channel for the troposphere and far UV ($\lambda > 300$ nm) channel for the stratosphere.

The solution of transfer equation for time-gated return signal $I(\lambda_i, h)$ for the set of wavelengths λ_i, $i = 1, 2...$, is sought in the framework of plane-stratified atmospheric model, that is the optical characteristics of the atmosphere are piecewise constant functions of the height h. The atmosphere is divided into n_h layers with non-uniform step (chosen to be shorter within cloud layers and aerosol inversions). In each layer Δh_j the model values of ozone concentration $N_{O_3}(h)$ for midlatitude summer, aerosol and molecular scattering coefficients, and scattering phase functions are specified in tabular form, respectively, using data from Refs. 39, 2, 29, and 40. The O_3 absorption cross sections in the UV at temperature 229 K are those from Ref. 22. The optical parameters of cirrus clouds are taken from Ref. 41 for model of randomly oriented hexagonal columns of a medium size.

The $I(\lambda_i, h_j)$ quantity is calculated for the initial and boundary conditions corresponding to real experiments[12,30,34,37]; in particular, divergence angle of the laser beam was set to $\varphi_s = 0.1$ mrad, while the total field of view (FOV) angle of the receiving telescope varied in the range $\varphi_d = 0.2–1$ mrad.

3. Model $N_{O_3}(h)$ estimates under conditions of multiple scattering background and deficient *a priori* information

Estimate of the vertical ozone profile $N_{O_3}(h)$ from single scattering signal at two wavelengths λ_1, λ_2, chosen from the condition of marked O_3 absorption, immediately follows from the DIAL method (4)

$$N_{O_3}(h) = \frac{1}{2\Delta K}\left[\frac{d}{dh}\ln R_\lambda(h) + A + B\right], \qquad (9)$$

where

$$R_\lambda(h) = P(\lambda_1,h)/P(\lambda_2,h)\,. \qquad (10)$$

As was already noted above, under conditions of real turbid or cloudy atmosphere, the effects of second-order elastic scattering at working wavelengths will add, to the flux incident on the photodetector, an additional systematic positive quantity $\Delta I(\lambda_i, h)$, distorting the true value given by expression (10). As a result, equation (9) will assume the form for the profile $N_{O_3}(h)$ biased due to multiple scattering noise:

$$N_{O_3}(h) = \frac{1}{2K}\left\{\frac{d}{dh}\ln\left[R_\lambda(\lambda_1,\lambda_2,h)\chi(\lambda_1,\lambda_2,h\right] + A + B\right\}, \qquad (11)$$

where

$$\chi(\lambda_1,\lambda_2,h) = \frac{I(\lambda_1,h)/I(\lambda_2,h)}{I_0(\lambda_1,h)/I_0(\lambda_2,h)}\,. \qquad (12)$$

To examine the outlined method, we repeated the well-known[21] calculational estimates of the accuracy of $N_{O_3}(h)$ retrieval under conditions of extreme inhomogeneity in $\beta_a(h)$ and $\sigma_a(h)$ in the planetary boundary layer (PBL). The calculated results for two possible variants of elastic scattering are shown in Fig. 1.

They appear to be in a good agreement with the estimates by Kovalev and McElroy,[21] confirming strong influence of the $\beta_\pi(h)$ gradient on sensing results. As was already noted above, the use of Raman sensing channels[11,12,30] makes it possible to eliminate this error because in this case the quantity $A = 0$ in formulas (4) and (11). Accordingly,

$$\Delta K = \left[K(\lambda_1) - K(\lambda_2)\right]/2,$$

where λ_i are the wavelengths of Raman return signals. Figure 2 shows the of numerical results on

$N_{O_3}(h)$ in the lower troposphere under assumption of Raman differential absorption lidar with the parameters used in Ref. 30, that is, we use $\lambda_1 = 277.5$ and $\lambda_2 = 283.6$ nm corresponding to rotational-vibrational Raman transitions of O_2 and N_2 excited with the fourth harmonic of Nd : YAG laser.

Characteristically, the strong aerosol inversion (Fig. 2*a*, models of $\sigma_a(h)$) does not affect the accuracy of $N_{O_3}(h)$ retrieval in this case. However, for large angular apertures, such as $\varphi_d \approx 1$ mrad, quite noticeable influence of multiple scattering leading to bias of retrieved characteristic can occur.

The retrieved altitude profile of ozone concentration within the optically active atmosphere ($h = 0$–30 km) taking into account the multiple scattering effect are presented in Figs. 3 and 4.

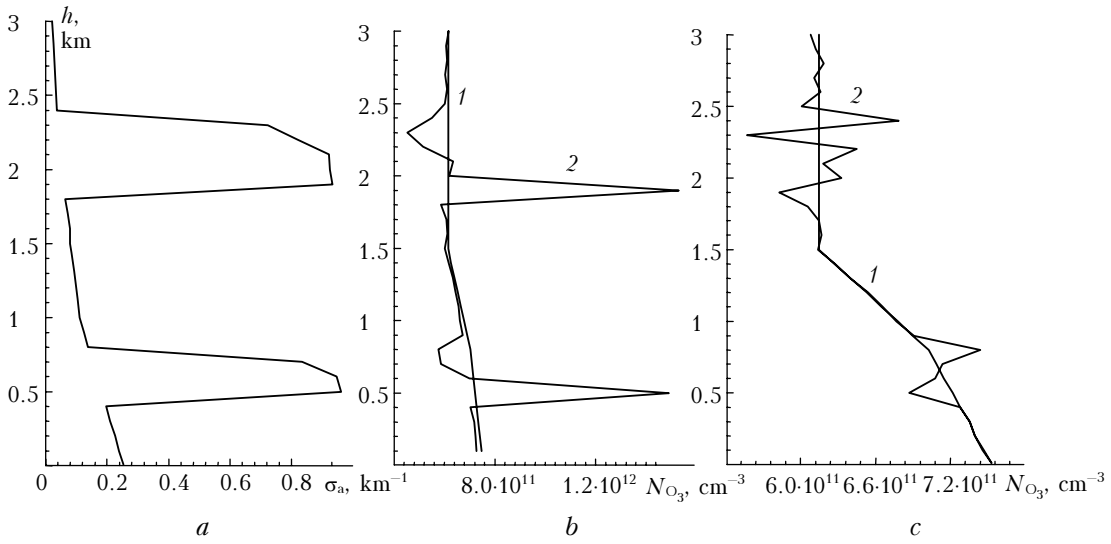

Fig. 1. Retrieval of the profile of ozone concentration in the presence of inversion layers according to data of DIAL sensing of elastic scattering: (*a*) profile of aerosol scattering coefficient; (*b*) data for lidar at $\lambda_1 = 292$, $\lambda_2 = 319$ nm; (*c*) results for lidar at $\lambda_1 = 308$ and $\lambda_2 = 315$ nm. Calculations were made for receiving angle $\varphi_d = 0.2$ mrad: model (curve *1*) and retrieved (*2*) profiles.

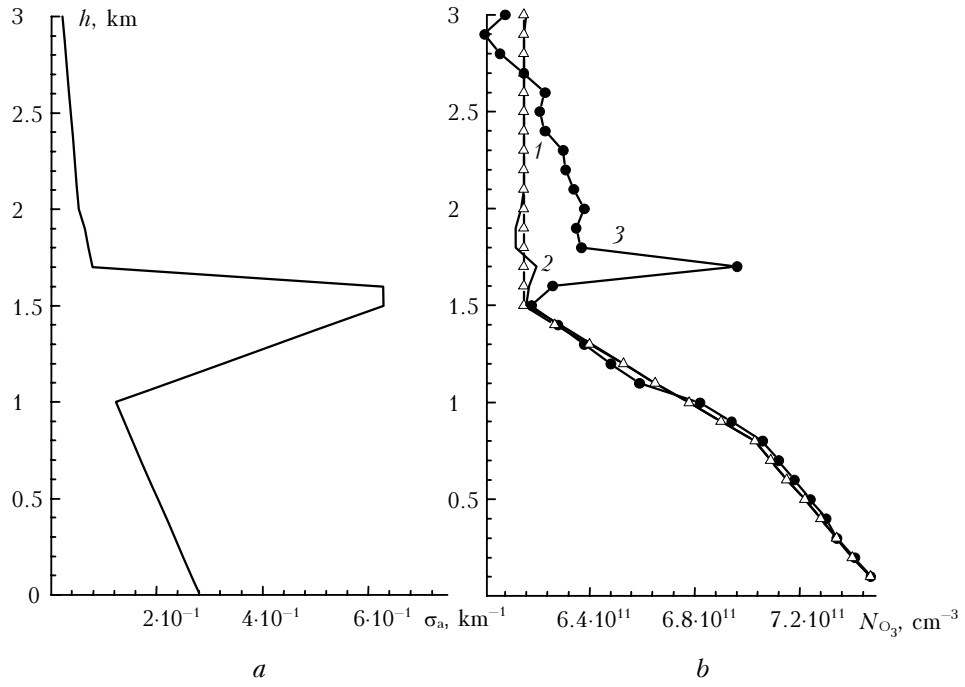

Fig. 2. Retrieval of the profile $N_{O_3}(h)$ by Raman lidar in the presence of inversion layer: (*a*) model profile $\sigma_a(h)$; (*b*) results for lidar at $\lambda_0 = 266$ (curve *1*), $\lambda_1 = 277.5$ (curve *2*), and $\lambda_2 = 283.6$ nm (curve *3*). Calculations used the angles $\varphi_d = 0.2$ and 1 mrad [(*2*) and (*3*)].

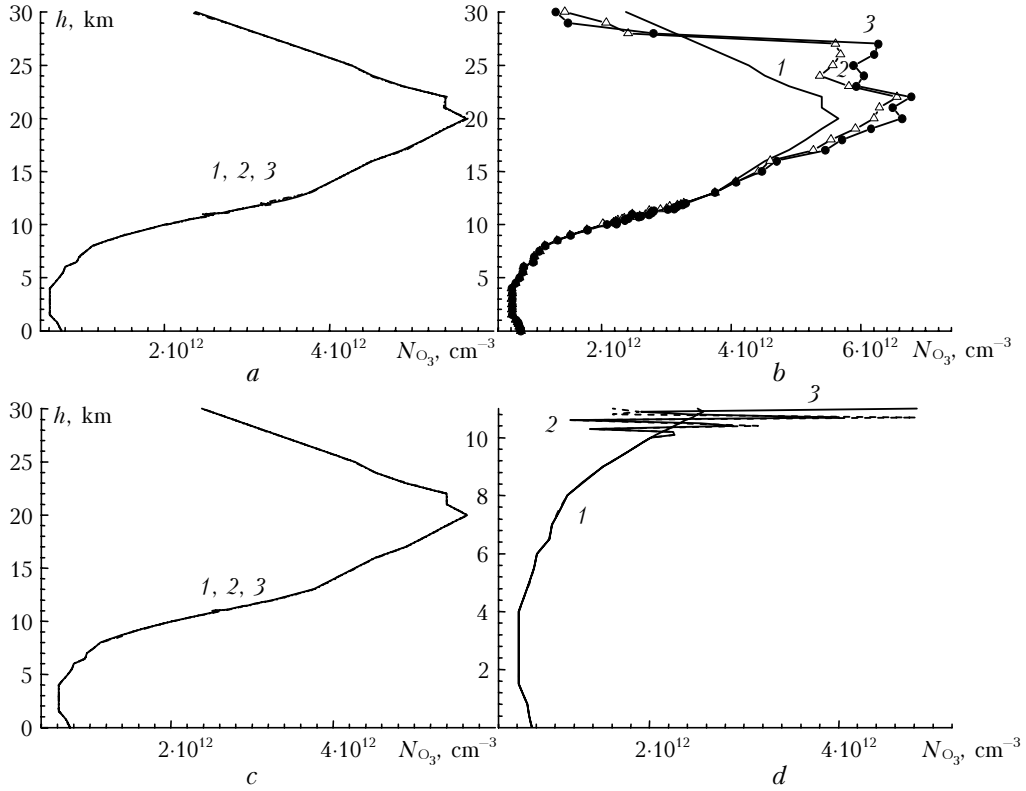

Fig. 3. The $N_{O_3}(h)$ retrieval by DIAL of Raman and elastic scattering in the altitude range h = 0–30 km under conditions of clean atmosphere: model profile (curve *1*); retrieved profiles according to the data for angles φ_d = 0.2 (curve *2*) and 1 mrad (curve *3*); (*a*) elastic scattering lidar at λ_1 = 308, λ_2 = 315 nm; (*b*) lidar at λ_1 = 292 and λ_2 = 319 nm; (*c*) and (*d*) Raman lidar at λ_0 = 308, λ_1 = 307, λ_2 = 332 nm and λ_0 = 266.5, λ_1 = 277, λ_2 = 283.6 nm.

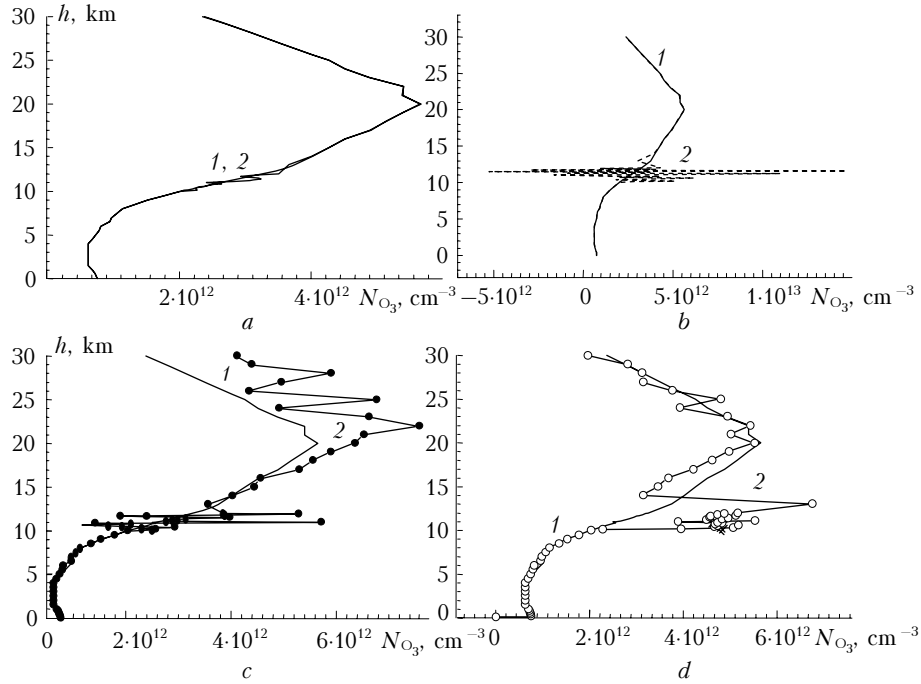

Fig. 4. Retrieval of ozone concentration profile from data acquired under cloudy atmospheric conditions at height h = 10–12 km, τ_{cl} = 0.1: (*a*) sensing by elastic scattering lidar at λ_1 = 308, λ_2 = 315 nm; (*b*) as for the above-indicated lidar except with τ_{cl} = 0.2; (*c*) results for lidar with λ_1 = 292, λ_2 = 319 nm; (*d*) sensing by RVRR lidar with λ_0 = 308, λ_1 = 307, λ_2 = 332 nm. Reception angle φ_d = 0.2 mrad. Shown are model (curve *1*) and retrieved (curve *2*) profiles $N_{O_3}(h)$.

Under conditions of clean atmosphere ("background" model[1,2]) and the appropriate choice of working wavelengths λ_i, the $N_{O_3}(h)$ estimate has minimum bias (Figs. 3*a* and *c*). We note that in Fig. 3*c* the estimates are obtained for a virtual prototype of rotational-vibrational Raman (RVVR) lidar (in terminology of the authors of Ref. 12). The specific feature of this lidar is that it uses as a reference wavelength (λ_{on}) the wavelength $\lambda_1 = 307$ nm corresponding to purely rotational spectrum of XeCl in the clean atmosphere ($N_2 + O_2$). We use as λ_{off} the rotational-vibrational spectra of nitrogen ($\lambda_2 = 332$ nm) or oxygen ($\lambda_2 = 323$ nm). If λ_{on} is chosen in the "dark" part of UV spectrum, then because of the relative weakness of the $I(\lambda, h)$ signal insignificant multiple scattering contributions $\Delta I_{ms}(\lambda, h)$ lead to a marked bias of the $N_{O_3}(h)$ estimate in the region of ozone layer (Fig. 3*b*). This conclusion exactly fits the practical recommendations.[24] If both of the wavelengths λ_{on} and λ_{off} lie in the "dark" part of UV (Fig. 3*d*), then violation of the solution is possible at the tropopause level only due to $\Delta I_{ms}(\lambda, h)$, at $h = 9$–11 km.

Figure 4 presents calculated results for most urgent situation of sensing under conditions of clean atmosphere in the presence weakly discernible cirrus clouds at altitudes $h = 10$–12 km. For the elastic backscatter DIAL ($\lambda_1 = 308$, $\lambda_2 = 315$ nm) the multiple scattering effects lead to insignificant $\Delta N_{O_3}(h)$ errors within optically thin cloud layer ($\tau_{cl} = 0.1$, Fig. 4*a*). Already after insignificant increase of the optical depth up to $\tau_{cl} \approx 0.2$ (Fig. 4*b*) the retrieval of O_3 concentration within the cloud layer becomes impossible. However, above the cloud the signal ratio $I(\lambda_1, h)/I(\lambda_2, h)$ returns to unperturbed values and ozone concentration profile can be retrieved with high accuracy (as can be seen from Fig. 4). For another wavelength pair of elastic scatter lidar with $\lambda_1 = 292$ and $\lambda_2 = 319$ nm (Fig. 4*c*) there is no possibility of retrieving ozone concentration profile not only within the cloud layer but also above it.

The latter is because the $I(\lambda_1, h)$ and $I(\lambda_2, h)$ signals have different multiple scattering contributions due to stronger ozone absorption at the wavelength λ_1. Due to the weak signal at $\lambda_1 = 292$ nm it is impossible to reach needed compensation for multiple scattering contribution in the ratio $I(\lambda_1, h)/I(\lambda_2, h)$. For this same reason, the results presented in Fig. 3*b* are unsatisfactory; in addition they indicate that the wavelengths combination is incorrect.

Next, Fig. 4*d* shows the results of retrieval of O_3 concentration using Raman lidar with the wavelengths $\lambda_0 = 308$, $\lambda_1 = 307$, and $\lambda_2 = 332$ nm. The intensity of Raman backscatter is 3–4 orders of magnitude lower than the elastic scattering signal; in addition, it is further reduced due to cloud screening.[33] This leads to a marked influence of secondary scattering processes in the presence of larger absorption at one of the wavelengths. The numerical experiment in this case yielded unsatisfactory result of $N_{O_3}(h)$ retrieval.

Characteristically, the multiple scattering effect within the anomalous aerosol layers is markedly weaker even when they have optical depths comparable with the cloud layers. Such optical depths are possible in scenario of emission of volcanic material into the stratosphere. This is well known[1,11] effect, associated with larger asymmetry of scattering phase function of cloud crystals than aerosol particles.

Figure 5*b* shows possible $\Delta N_{O_3}(h)$ variations in the region of the stratosphere due to multiple scattering of elastic scattering signals at the wavelengths $\lambda_1 = 308$ and $\lambda_2 = 353$ nm. The profiles $\sigma_a(h)$ for the stratosphere in post-volcanic time intervals are taken from Ref. 19 and reproduced in Fig. 5*a*.

We note, in particular, that the $\Delta N_{O_3}(h)/N_{O_3}(h)$ values presented in Ref. 19 are in a good qualitative agreement with our estimates; however their too high level seems to be insufficiently justified. The numerous results of complex $N_{O_3}(h)$ measurements, systematized, e.g., in Refs. 17, 18, and 30 do not support such pessimistic estimates either.

On the other hand, this same Reference 19 reasonably notes that the significant source of $N_{O_3}(h)$ measurement error may be temperature dependence of the ozone cross section $K(\lambda) = K(\lambda, T)$ (where T is the temperature), becoming most significant in satellite laser sensing, with its usual coverage of considerable latitudinal and seasonal variation of temperature ΔT. Indeed, the known experimental data[42] suggest that for T in the range 205–295 K, the variations $\Delta K(\lambda, T)/K(\lambda, T)$ are 50–60% at $\lambda = 310$ nm and reach 200% at $\lambda = 320$ nm. It is noteworthy that in the cold Huggins bands, the dependence $K(\lambda, T)$ may be extreme. In our estimates presented in Fig. 5*c* we assumed the constant bias

$$\Delta K(\lambda, T) = \pm 0.4 K(\lambda, T),$$

where, in accordance with Ref. 22, $T_0 = 229$ K, in finite altitude range $h = 15$–24 km. The comments are quite obvious. Unfortunately, in most of the above-mentioned references dealing with systematic $N_{O_3}(h)$ monitoring, the possible influence of temperature inversions is neglected, as well as the effect of multiple scattering. The method of temperature corrections of ozone cross sections is rather well developed.[42,43] In particular, for $\lambda_1 = 308$ nm, i.e., the wavelength of XeCl laser radiation and also the most popular wavelength in the framework of DIAL method, Brion et al.[43] propose the complex empirical formula

$$K_{308}(T) = 1.15 + 288.2 \exp(-2143/T) \quad \left[10^{-19}\ \text{cm}^{-2}\right].$$

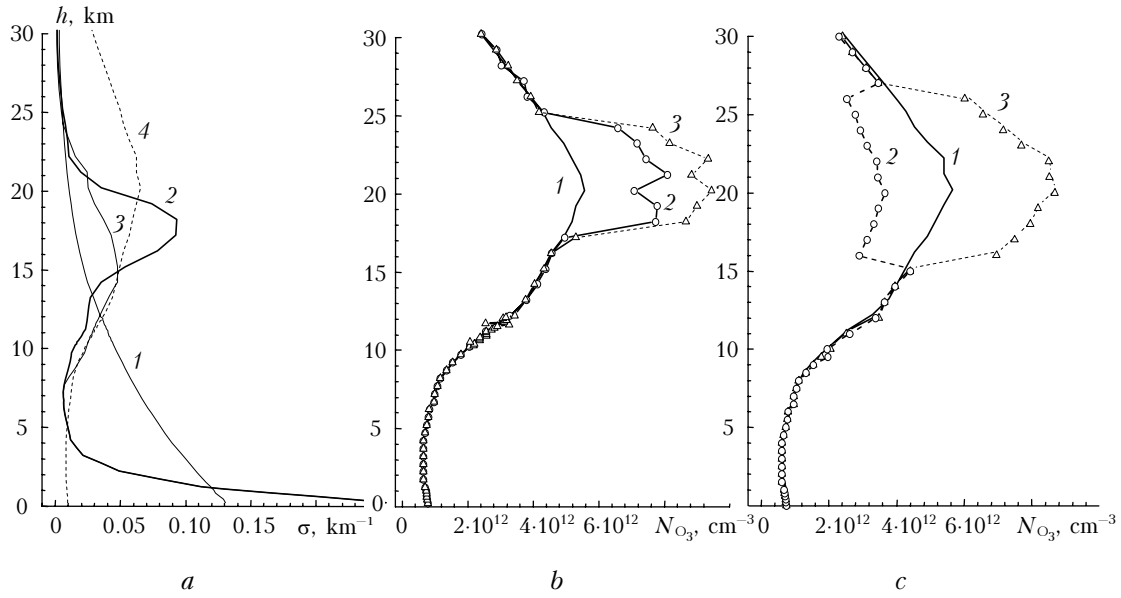

Fig. 5. The $N_{O_3}(h)$ retrieval in the elastic scattering lidar sensing at $\lambda_1 = 308$, $\lambda_2 = 353$ nm in the presence of aerosol or temperature inversions in the stratospheric height interval: (*a*) model profiles of the coefficients of molecular scattering $\sigma_R(h)$ (curve *1*); aerosol extinction $\sigma_a(h)$ (curves *2* and *3*); and ozone absorption σ_{O_3} (curve *4*); (*b*) model profile $N_{O_3}(h)$ (curve *1*); and the profiles retrieved for the corresponding profiles $\sigma_a(h)$ (curves *2* and *3*); and (*c*) modeled and retrieved profiles of ozone concentration (curves *1*, *2*, and *3*) for increased (curve *2*) and decreased (curve *3*) temperatures.

However, this obviously calls for simultaneous sensing of the vertical temperature profile $T(h)$, the problem also successfully solved at a number of lidar stations[16,17] through involvement of additional Raman scattering channels.

Conclusion

We have presented the results of numerical experiments aimed at evaluating the well known differential absorption lidar methods under conditions of active interference from multiple scattering noise. All the known DIAL methods are based on the use of single scattering signals. The idea of the numerical experiment was to substitute the "real signals" in the well known inversion formulas. It was found that the multiple scattering effects in sensing of atmospheric ozone in the UV wavelength range in the presence of broken clouds or inversions of aerosol loading become comparable with other error sources. Sizable reduction of multiple scattering noise can be reached through optimal choice of sensing wavelengths. Based on our estimates, this is the pair of wavelengths of elastic scattering, namely $\lambda_1 = 308$ and $\lambda_2 = 315$ nm. The inelastic (Raman) DIAL sensing technique, developed in a number of recent publications,[11,12] appears to be less stable to multiple scattering background, especially in the region of the stratosphere. At the same time, we arrive at the conclusion that the additional Raman channel can be useful for separation of aerosol and molecular scattering components and for synchronous estimate of vertical temperature profile. The neglect of temperature dependence of the absorption cross section may lead to uncontrolled bias of the results and may be the reason for time trends in vertical stratification of stratospheric ozone.

Appendix

Iteration method of separation of optical variables

We will consider the case of two-frequency sensing, with $i = 1, 2$. Main equation (1) will be written in the following discrete form:

$$S(\lambda_i,h_j) = \beta_\pi(\lambda_i,h_j)T^2(\lambda_i,h_{j-1})T^2(\lambda_i,\Delta h_j),\ j = 0,1,2,3,\cdots, \tag{A1}$$

where

$$S(\lambda_i,h_j) = \frac{P(\lambda_i,h_j)h_j^2}{P_0(\lambda_I)\xi(h_j)},\ \ \Delta h_j = h_j - h_{j-1};$$

$$T^2(\lambda_i,h_j) = \exp\left\{-2\int_{h_0}^{h_j}\sigma(h')\mathrm{d}h'\right\},$$

$$T^2(\lambda_i,\Delta h_j) = \exp\left\{-\Delta h_j\left[\sigma(h_{j-1}) + \sigma(h_j)\right]\right\}.$$

In an identical way, equation (A1) becomes

$$S(\lambda_i,h_j) = S(\lambda_i,h_{j-1})\frac{\beta_\pi(\lambda_i,h_j)}{\beta_\pi(\lambda_i,h_{j-1})}T^2(\lambda_i,\Delta h_j). \tag{A2}$$

This discrete formulation of lidar equation does not contain transmission functions $T^2(\lambda_i,h_{j-1})$ in explicit form, thus allowing one to work with signals in arbitrary (comparable at a single wavelength) units. Next, we naturally use the following representations

$$\beta_\pi(\lambda_i,h) = \beta_a(\lambda_i,h) + \beta_m(\lambda_i h); \quad (A3)$$

$$\sigma(\lambda_i,h) = \sigma_a(\lambda_i,h) + \sigma_m(\lambda_i,h), \quad (A4)$$

where subscripts "a" and "m" denote, respectively, the aerosol and molecular components. Finally, we assume that

$$\beta_a(\lambda_i,h) = q_j\beta_a(\lambda_i,h_{j-1}). \quad (A5)$$

Formula (A5) implicitly suggests that $q_j(\lambda_1) = q_j(\lambda_2)\, q_j(\lambda_1) = q_j(\lambda_2)$, i.e., it is assumed that refractive indices of aerosol particles $m(\lambda_1) \cong m(\lambda_2)$ and the relative particle size spectra $f(\rho, \lambda_1) \cong f(\rho, \lambda_2)$, where $\rho = 2\pi r/\lambda$ (r is particle radius). Such an approach as a means of reduction of the amount of unknowns in (A2) is not quite correct for usual scheme of multifrequency sensing of the aerosol atmosphere.[27,28] However, for DIAL measurements, usually taken at very close wavelengths, assumption (A5) is quite justified and allows one to solve system (A2) straightforwardly. Indeed, taking into account Eqs. (A3) – (A5), system (A2) modifies to

$$\begin{cases} q_j\beta_a(\lambda_1,h_{j-1}) + \beta_m(\lambda_1,h_j) = F_{1,j}, \\ q_j\beta_a(\lambda_2,h_{j-1)}) + a(\lambda_1\lambda_2)\beta_m(\lambda_1,h_j) = F_{2,j}, \end{cases} \quad (A6)$$

where

$$a(\lambda_1,\lambda_2) = (\lambda_1/\lambda_2)^4;$$

$$F_{i,j} = \frac{S(\lambda_i,h_j)\beta_\pi(\lambda_i,h_{j-1})}{S(\lambda_i,h_{j-1})T^2(\lambda_i,\Delta h_j)} \quad (A7)$$

are measured functionals at the wavelengths λ_i, $i = 1, 2$. With optical characteristics $\beta_\pi(\lambda_i,h_0)$ assumed known at the initial point h_0 (the algorithm allows the reverse recursion in any direction), for the remaining unknowns $\beta_m(\lambda_i,h_j)$ and q_j it trivially follows that

$$q_j = \frac{a(\lambda_1,\lambda_2)F_{1,j} - F_{2,j}}{a(\lambda_1,\lambda_2)\beta_a(\lambda_1,h_{j-1}) - \beta_a(\lambda_2,h_{j-1})}; \quad (A8)$$

$$\beta_m(\lambda_1,h_j) = F_{1,j} - q_j\beta_a(\lambda_1,h_{j-1}). \quad (A9)$$

For small height bins Δh_j it is additionally assumed[27,28] in Eq. (A7) that $T(\Delta h_j) \cong 1$. However, in the UV wavelength range, where $T(h)$ are substantial, this may lead to accumulation of error. It is preferable to conserve $T(\Delta h_j)$ in Eq. (A7) and estimate them using any appropriate model such as suggested by Elterman.[29] We note that the accuracy and applicability limits of the method can be improved by use of additional information on vertical profile of aerosol scattering phase function $g_a(\lambda,h)$. Moreover, as was shown earlier,[28] it is not required to be specified too accurately. In this case, there appears a possibility of solving system (A6) in the complete form:

$$\begin{cases} q_j\beta_a(\lambda_1,h_{j-1}) + \beta_m(\lambda_1,h_j) = \\ = F'_{1,j}\exp\left\{\Delta h_j\left[\dfrac{\beta_m(\lambda_1,h_j)}{g_m} + \dfrac{q_j\beta_a(\lambda_1,h_{j-1})}{g_a(\lambda_1,h_j)}\right]\right\} \\ q_j\beta_a(\lambda_2,h_{j-1}) + a(\lambda_1,\lambda_2)\beta_m(\lambda_1,h_j) = \\ = F'_{2,j}\exp\left\{\Delta h\left[\dfrac{a(\lambda_1,\lambda_2)\beta_m(\lambda_1,h_j)}{g_m} + \dfrac{q_j\beta_a(\lambda_2,h_{j-1})}{g_a(\lambda_2,h_j)}\right]\right\} \end{cases}, \quad (A10)$$

where

$$F'_{i,j} = \frac{S(\lambda_i,h_j)\beta_\pi(\lambda_i,h_{j-1})}{S(\lambda_i,h_{j-1})}\exp\left\{\Delta h\left[\frac{\beta_m(\lambda_i,h_{j-1})}{g_m}\right]\right\};$$

$g_m = 3/8\pi$ is the molecular scattering phase function, $g_a = 0.03$, in the region of the stratosphere.[2]

Solution of Eq. (A10) for q_j and $\beta_m(\lambda_i,h_j)$ can be constructed with the help of iteration algorithm developed in Refs. 25 and 28.

References

1. G.M. Krekov, and M.M. Krekova, Atmos. Oceanic Opt. **18**, Nos. 5–6, 422–431 (2005).
2. G.M. Krekov and S.G. Zvenigorodsky, *Optical Model of the Middle Atmosphere* (Nauka, Novosibirsk, 1990), 280 pp.
3. V.V. Zuev, A.V. Elnikov, and V.D. Burlakov, *Laser Sensing of the Middle Atmosphere* (Rasko, Tomsk, 2002), 352 pp.
4. M. Natajan, J. Geophys. Res. D **91**, No. 1, 1153–1166 (1986).
5. D.W. Rush and R.S. Ekman, J. Geophys. Res. **90**, 12991–12998 (1985).
6. *2nd International Laser Radar Conf. (ILRC 2004)*, Proc. Matera (Italy, 2004), 575 pp.
7. J. Leleveld and P.J. Crutzen, Nature (Gr. Brit.) **343**, 227–233 (1990).
8. J.E. Jonson and I.S. Isaksen, J. Atmos. Chem. **16**, 99–122 (1993).
9. J. Reichardt, A. Ansmann, M. Serwasi, C. Weitkamp, and W. Michaelis, J. Geophys. Res. **23**, 1929–1932 (1996).
10. S.R. Pal and L.R. Bissonette, Appl. Opt. **37**, No. 27, 6500–6511 (1996).
11. J. Reichardt, Appl. Opt. **39**, No. 33, 6058–6071 (2000).
12. J. Reichardt, S.E. Bisson, S. Reichardt, C. Weitkamp, and B. Neidhart, Appl. Opt. **39**, No. 33, 6072–6079 (2000).

13. R.M. Schotland, in: *Proc. Third Symp. on Remote Sensing of the Environment* (Michigan, Ann. Arbor., USA, 1964), pp. 215–224.
14. V.E. Zuev, *Laser Beam in the Atmosphere* (Plenum Publ. Corp., New York, 1981), 345 pp.
15. A.J. Gibson and L. Thomas, Nature (Gr. Brit.) **256**, No. 5578, 561–563 (1975).
16. V. Mattias, J. Bosenberg, V. Frendenthaler, A. Amadeo, D. Balis, and A. Chaikovsky, Appl. Opt. **43**, 961–976 (2004).
17. S. Godin, A.I. Carswell, D.P. Donovan, H. Claude, and W. Steibrecht, Appl. Opt. **38**, No. 30, 6225–6236 (1999).
18. L. Fiorani and E. Durieux, Opt. and Laser Technol. **33**, 371–377 (2001).
19. O. Uchino, M.P. McCormic, T.J. Swissler, and L.R. McMaster, Appl. Opt. **25**, No. 21, 3946–3951 (1986).
20. E.V. Browell, S. Ismail, and T. Shipley, Appl. Opt. **24**, 2827–2836 (1985).
21. V.A. Kovalev and J.L. McElroy, Appl. Opt. **33**, 8393–8401 (1994).
22. O.K. Kostko, V.S. Portasov, V.U. Khattatov, and E.A. Chayanova, *Application of Lasers for Determination of Atmospheric Composition* (Gidrometeoizdat, Leningrad, 1983), 216 pp.
23. D. Kedar and S. Arnon, Appl. Opt. **44**, No. 6, 984–992 (2005).
24. V.S. Bukreev, S.K. Vartapetov, and I.A. Veselovsky, Kvant. Elektron. **21**, No. 6, 591–596 (1994).
25. V.E. Zuev, G.M. Krekov, I.E. Naats, and V.N. Skorinov, Izv. Akad. Nauk SSSR, Ser. Fiz. Atmos. Okeana **12**, No. 12, 1326–1329 (1975).
26. V.E. Zuev, G.M. Krekov, M.M. Krekova, and I.E. Naats, *Theoretical Aspects of the Problem of Atmospheric Laser Sensing* (Nauka, Novosibirsk, 1976), pp. 3–33.
27. A. Cohen and V.E. Derr, in: *Conf. Atmosph. Radiation* (Amer. Meteorol. Soc., Boston, 1972), pp. 301–306.
28. G.M. Krekov, *Remote Methods of Atmospheric Study* (Nauka, Novosibirsk, 1980), pp. 3–40.
29. L. Elterman, Environ. Res. Papers (1968), No. 285, 50 pp.
30. B. Lazzarotto, M. Friound, and G. Larcheveque, Appl. Opt. **40**, No. 18, 2985–2997 (2001).
31. R. Measures, *Laser Remote Sensing* (John Wiley & Sons, New York, 1984).
32. A. Ben-David, Appl. Opt. **34**, 2802–2810 (1995).
33. G.M. Krekov and M.M. Krekova, Atmos. Oceanic Opt. **17**, No. 10, 745–752 (2004).
34. A. Papayannis, G. Ancellet, J. Pelon, and G. Megie, Appl. Opt. **29**, No. 4, 467–476 (1990).
35. V. Simeonov, B. Calpini, and H. Van der Bergh, in: *Proc. of 21 Conf. on Lidar Remote Sensing in Atmosph. and Earth* (Quebec, Canada, 2002), pp. 19–22.
36. R.V. Ussushkin, J.F. Hahn, A. Carswell, and A. Ulitsky, in: *Proc. of 21 Conf. on Lidar Remote Sensing in Atmosph. and Earth* (Quebec, Canada, 2002), pp. 185–188.
37. M.H. Proffit and A.O. Langford, Appl. Opt. **36**, No. 12, 2568–2585 (1997).
38. J.A. Sunesson, A. Apituley, and D.P. Swart, Appl. Opt. **33**, No. 30, 7045–7058 (1994).
39. B.A. Fomin and Yu.V. Gershanov, *Tables of the Benchmark Calculations of Atmospheric Fluxes for the ICRCCM Test Cases* (Rus. Res. Center "Kurchatov Institute": IAE-5981/1, Moscow, 1996), 52 pp.
40. G.M. Krekov and R.F. Rakhimov, *Optical Models of Atmospheric Aerosol* (Publishing House of Tomsk Affiliate of Siberian Branch of USSR Academy of Sciences, Tomsk, 1986), 295 pp.
41. G.M. Krekov, M.M. Krekova, and D.N. Romashov, Izv. Vyssh. Uchebn. Zaved., Ser. Fizika **44**, No. 11, 56–66 (2001).
42. J. Malicet, D. Doumont, J. Charbonnier, C. Parisse, A. Chakir, and J. Brion, J. Atmos. Chem. **21**, 263–273 (1995).
43. J. Brion, A. Chakir, D. Daumont, J. Malicet, and C. Parisse, Chem. Phys. Lett. **213**, 610–612 (1993).